Selenium(IV) uptake by maghemite (γ-Fe2O3)

ARTICLE *in* ENVIRONMENTAL SCIENCE & TECHNOLOGY · JANUARY 2014

Impact Factor: 5.33 · DOI: 10.1021/es4045852 · Source: PubMed

6 AUTHORS, INCLUDING:

Norbert Jordan
Helmholtz-Zentrum Dresden-Rossendorf
16 PUBLICATIONS **158** CITATIONS
SEE PROFILE

Andreas C Scheinost
Helmholtz-Zentrum Dresden-Rossendorf
179 PUBLICATIONS **4,391** CITATIONS
SEE PROFILE

Environmental Science & Technology

Article

pubs.acs.org/est

Selenium(IV) Uptake by Maghemite (γ-Fe_2O_3)

Norbert Jordan,[†,*] Aline Ritter,[†] Andreas C. Scheinost,[†,‡,*] Stephan Weiss,[†] Dieter Schild,[§] and René Hübner[∥]

[†]Institute of Resource Ecology, Helmholtz-Zentrum Dresden-Rossendorf e.V., 01328 Dresden, Germany

[‡]The Rossendorf Beamline at ESRF, P.O. Box 220, F-38043 Grenoble, France

[§]Institute for Nuclear Waste Disposal, Karlsruhe Institute for Technology, Hermann-von-Helmholtz-Platz 1, 76344 Eggenstein-Leopoldshafen, Germany

[∥]Institute of Ion Beam Physics and Materials Research, Helmholtz-Zentrum Dresden-Rossendorf e.V., Bautzner Landstrasse 400, 01328 Dresden, Germany

Supporting Information

ABSTRACT: The mechanism of selenium(IV) uptake by maghemite was investigated on both the macroscopic and the molecular level. Maghemite nanoparticles exhibited fast adsorption kinetics toward selenium(IV). Batch experiments showed a decreased sorption with increasing pH (3.5−11). Ionic strength variations (0.01 to 0.1 M NaCl) had no significant influence on selenium(IV) uptake. Electrophoretic mobility measurements revealed a significant shift toward lower values of the isoelectric point of maghemite upon selenium(IV) uptake, suggesting the formation of inner-sphere surface complexes. At the molecular level, using X-ray Absorption Fine-Structure Spectroscopy (EXAFS), the formation of both bidentate binuclear corner-sharing (^{2}C) and bidentate mononuclear edge-sharing (^{1}E) inner-sphere surface complexes was observed, with a trend toward solely ^{1}E complexes at high pH. The absence of a tridentate surface complex as observed for arsenic(III) and antimonite(III) might be due to the relatively small size of the $Se^{IV}O_3$ unit. These new spectroscopic results can be implemented in reactive transport models to improve the prediction of selenium migration behavior in the environment as well as its monitoring through its interaction with maghemite or maghemite layers at the surface of magnetite. Due to its chemical stability even at low pH and its magnetization properties allowing magnetic separation, maghemite is a promising sorbing phase for the treatment of Se polluted waters.

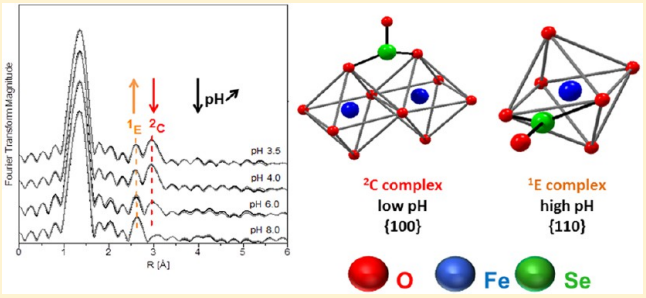

INTRODUCTION

Although Se is an essential element for animals and humans,[1] it is toxic in excess.[1−3] A teratogenic effect and poisoning (birth deformity and mortality) of fish and wildlife were observed at Kesterson National wildlife refuge in California.[4−6] Selenium-79, a long-lived ($t_{1/2} \approx 3.27 \times 10^5$ years[7]) and radiotoxic radionuclide present in spent nuclear fuel, is of high relevance in the context of nuclear waste management, according to safety assessments.[8−10] Although the most important exposure route to Se for humans is food,[1,11] selenium leads to severe health effects when present even at low concentrations in drinking water.[12,13]

Adsorption and heterogeneous reduction on iron, alumina, titanium oxides, and so forth were shown to be mechanisms able to retard the migration of selenium in the environment.[14−17] Maghemite, the red-brown γ polymorph of Fe_2O_3, also belongs to the wide range of naturally occurring iron oxides. It is found in tropical and subtropical soils, and is commonly formed from the oxidation of lithogenic magnetite.[18−21] Other reported formation pathways are the dehydroxylation of lepidocrocite or heating of goethite in the presence of organic matter.[18] It was also identified as a corrosion product of steel waste canisters[22] and iron archeological analogues.[23−25]

Recently, nanomagnetite particles (10−20 nm) were shown to be very promising sorbents for the removal of selenite from aqueous solutions, with a final concentration less than 5 μg L^{-1},[16,26] thus below the concentration recommended by the World Health Organization. The process responsible for these low concentrations is the reduction of Se(IV) to Se(−II) by magnetite and subsequent precipitation of highly insoluble FeSe.[16] However, such nanomagnetite particles are transformed to maghemite either by aerial oxidation or by interfacial ionic and/or electron transfers depending on the pH.[27] Indeed, magnetite is thermodynamically unstable with respect to maghemite (γ-Fe_2O_3) and is slowly oxidized to maghemite even at room temperature in the presence of oxygen.[28] As already stated by Tang et al.[28] and Morin et al.,[29] the oxidation of magnetite to maghemite is therefore a process of high

Received: October 13, 2013
Revised: January 14, 2014
Accepted: January 14, 2014
Published: January 14, 2014

environmental significance. Consequently, decontamination processes of air equilibrated waters dealing with magnetite nanoparticles may in fact also involve coating layers of maghemite, which will in turn control the reactivity at the solid−water interface.[29]

Recently, the ability of maghemite nanoparticles to remove pollutants like Se(VI), Mo(VI), As(V), Cr(VI), Ni(II), Cu(II), and dyes from waters and waste waters was shown.[30−37] While selenium(IV) has been shown to sorb predominantly by formation of inner-sphere complexes at the surface of a range of iron, aluminum, titanium, and manganese oxides,[15,38−41] the selenium(IV) retention mechanism by maghemite (γ-Fe_2O_3) was so far never thoroughly investigated.

Thus, in this study, we combined both macroscopic and spectroscopic measurements to elucidate the mechanisms of selenium(IV) sorption onto maghemite. Macroscopic investigations included batch sorption experiments and electrophoretic mobility measurements. The selenium(IV) surface speciation, i.e., the nature of the sorbed species and their distribution at the solid−water interface, needed for the determination of thermodynamic surface complexation constants, was investigated and identified at the molecular level by performing X-ray Absorption Fine-Structure Spectroscopy (EXAFS) measurements.

EXPERIMENTAL SECTION

Solid Phase. Maghemite (γ-Fe_2O_3) was purchased from Alfa Aesar, with a high purity (>99.0%). Minor contamination by Na, Si, Mn, Ni, Cu, and Zn (<0.05% w/w) was evidenced by ICP-MS after digestion of maghemite. Specific surface area of maghemite was determined to be 38 $m^2\ g^{-1}$.[33] Maghemite was also characterized by X-ray diffraction, IR spectroscopy, and Mössbauer spectroscopy, which showed the presence of a well-crystallized solid, with no trace of other iron oxide compounds like goethite, hematite, or magnetite.[33] However, small traces of Fe(II) (<0.9% w/w) were determined photometrically by the 1.1 Phenanthroline method, but could not be detected by Mössbauer spectroscopy.[33] The uppermost layers of maghemite were investigated by X-ray Photoelectron Spectroscopy (XPS). Results showed no major impurities at the surface of maghemite and the impurities evidenced by ICP-MS were not confirmed by XPS, suggesting their presence in the bulk of the material. Using XPS, the $Fe(II)/Fe_{TOT}$ ratio on the surface of maghemite was found to be well below 3%, which is in the range of the analytical uncertainty (more details available in the Supporting Information, SI). Finally, to locally analyze the microstructure and in particular the morphology of the maghemite nanoparticles, transmission electron microscopy (TEM) investigations were performed (see details in the SI).

Sorption and Electrophoretic Mobility Experiments. Detailed information about reagents, sorption, and electrophoretic experiments can be found in the SI. In summary, to determine the time needed to reach the sorption equilibrium, experiments with increasing contact times up to 170 h were carried out (m/v = 0.25 g L^{-1}, I = 0.1 M NaCl, and $[Se^{IV}] = 5 \times 10^{-5}$ M). The pH of the suspensions was adjusted to 4.0 throughout these experiments. Uptake of selenium(IV) onto maghemite was studied from pH 3.5 to 11, at constant selenium(IV) concentration (5×10^{-5} M) and ionic strength (I = 0.1 M). The impact of the ionic strength on selenium(IV) uptake was also investigated, by using a background electrolyte concentration of 0.01 M of NaCl ($[Se^{IV}] = 5 \times 10^{-5}$ M). During our experiments, Hydride Generation-Atomic Absorption Spectrometry evidenced the absence of homogeneous reduction of selenium(IV) in the aqueous phase (see SI).

XAS Measurements. Selenium K-edge XANES (X-ray Absorption Near-Edge Structure) and EXAFS spectra were collected at the Rossendorf Beamline at ESRF (Grenoble, France). The energy of the X-ray beam was tuned by an Si(111) double-crystal monochromator operating in channel-cut mode. Two platinum-coated Si mirrors before and after the monochromator were used to collimate the beam into the monochromator and to reject higher harmonics. A 13-element high purity germanium detector (Canberra) together with a digital signal processing unit (XIA) was used to measure samples in fluorescence mode.

Samples with pH values from pH 3.5 to 8.0 were prepared under CO_2-free conditions by reacting 250 mg of maghemite (to get sufficient maghemite material for XAS analysis) with selenium(IV), at the same experimental conditions used during batch experiment but only at I = 0.1 M NaCl. After 3 days of stirring to reach sorption equilibrium, the samples were ultracentrifuged during 30 min at 187 000g. The wet pastes were transferred into sample holders, which were covered with Kapton tape and flash-frozen in liquid N_2. Great care was taken to exclude O_2 during sample transport and storage by keeping them in liquid N_2. At the beamline, they were rapidly (2 min) transferred to a closed-cycle He cryostat (with a large fluorescence exit window and a low vibration level (CryoVac), where they were kept at 15 K during the XAS measurements. As was confirmed by comparing repetitive short (10 min) XANES scans, the cooling prevented photon-induced redox reactions of the samples. For energy calibration, a gold foil (K-edge at 11919 eV) was chosen because of its greater inertness in comparison to Se. Data in the XANES region were collected in steps of 0.5 eV, i.e., with higher resolution than the resolution of the Si(111) crystal at the given vertical divergence (1.7 eV) and the broadening due to the core-hole lifetime (2.3 eV). A comparison of single scans of the same sample showed an accuracy of better than 0.5 eV. Dead time correction of the fluorescence signal, energy calibration, and the averaging of single scans were performed with the software package SixPack.[42] Normalization, transformation from energy into k space, and subtraction of a spline background was performed with WinXAS using routine procedures.[43] Shell-fit of EXAFS data was performed with WinXAS using theoretical back-scattering amplitudes and phase shifts calculated with FEFF 8.2.[44] The EXAFS data were also analyzed using the statistical software package ITFA[45] and with Morlet wavelets.[46]

RESULTS AND DISCUSSION

Time-Dependence Study. The uptake of selenium(IV) was completed within 24 h (SI Figure S1) and remained unchanged for longer contact times. Adding a safety margin of 100% and for convenient reasons, an equilibration time of 2 days was chosen for all further sorption experiments onto maghemite.

Sorption Edges and Ionic Strength Influence on Selenium(IV) Sorption. Selenium(IV) uptake onto maghemite strongly decreased with pH of the suspension (Figure 1). This behavior is typical for anion sorption to iron oxides.[47−49] The data presented in Figure 1 show that there is still a significant amount of selenium(IV) sorbed onto maghemite at pH values greater than the pH_{IEP} (~8.3), where the surface is negatively charged. Similar observations were also reported for iron oxides,[50,51] as well as for water-washed manganese nodule

dx.doi.org/10.1021/es4045852 | Environ. Sci. Technol. 2014, 48, 1665−1674

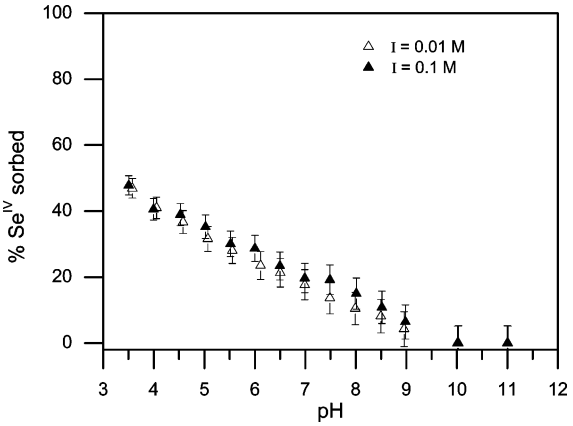

Figure 1. Selenium(IV) sorption edges onto maghemite at two different ionic strengths in NaCl (0.1 and 0.01 M). $[Se^{IV}]$initial = 5×10^{-5} M, m/v = 0.25 g L^{-1}, 2 days of shaking.

leached residues,[52] where selenium(IV) sorption took place at pH values greater than the pH_{PZC} (point of zero charge).

According to Stumm et al.,[53] the free energy of adsorption is a combination of both chemical and electrostatic effects. This means that above pH_{IEP}, the chemical component dominates the electrostatic one.[50,51]

Ionic strength variation between 0.1 and 0.01 M had no significant effect on Se(IV) sorption (Figure 1), similar to previous studies on goethite,[41,54] amorphous iron oxyhydroxides,[41] hematite,[14,54] anatase,[55] and γ-Al_2O_3.[15] This macroscopic observation is commonly considered as an indication for inner-sphere complexation. As expected for an iron(III) oxide, the dissolution of maghemite can be considered as negligible, since the amount of iron released into the supernatant remained below 50 μg L^{-1} between pH 3.5 and 11, as determined by ICP-MS (data not shown).

Electrophoretic Mobility Measurements. The isoelectric point (pH_{IEP}) of maghemite was found to be at pH ≈ 8.3 (Figure 2), which is in agreement with recently reported values ranging from 6.8 to 8.3.[35,56−59]

After reaction with Se(IV), this pH_{IEP} was significantly shifted toward lower pH (Figure 2). At pH higher than 9.0, the zeta potential of maghemite is no longer affected by Se sorption

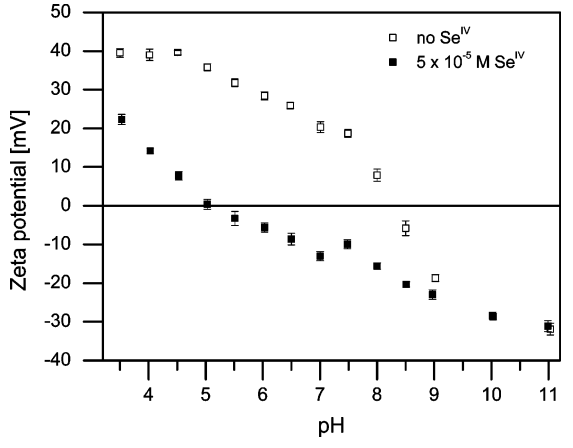

Figure 2. Zeta potential of maghemite before and after selenium(IV) sorption (m/v = 0.25 g L^{-1}, I = 0.1 M NaCl, $[Se^{IV}]_{initial} = 5 \times 10^{-5}$ M, 2 days of shaking).

(Figure 2), in agreement with batch sorption experiments (Figure 1).

The shift of the pH_{IEP} of mineral surfaces to lower values upon anion uptake, due to accumulation of negative charge within the shear plane, can be interpreted as inner-sphere coordination or surface precipitation. XAS showed no evidence for surface precipitates including iron(III) selenite phases (see XAS section below). Therefore, the formation of inner-sphere complexes is the most plausible explanation. Indeed, in parallel to spectroscopic investigations (EXAFS, FT-IR, Raman), the lowering of both pH_{IEP} and zeta potential values of mineral surfaces after sorption was considered to be an indication of inner-sphere complexation, e.g., after sorption of As(V) onto maghemite[58] and SeO_3^{2-} onto am-$Fe(OH)_3$ and γ-Al_2O_3.[15,41]

The results from batch experiments as well as electrophoretic mobility measurements strongly suggest that selenium(IV) forms inner-sphere complexes onto maghemite, i.e., the interaction proceeds via formation of chemical bonds. However, a spectroscopic characterization is mandatory for a detailed knowledge of the sorbed species at the solid/liquid interface at a molecular scale.

XAS Measurements. The Se K-edge XANES spectra of selenium(IV)-reacted maghemite samples (data not shown) are dominated by a strong white line at 12.662 keV, characteristic of the +IV oxidation state of selenium.[16] Since no additional shoulders at lower energy (12.656−12.657 keV) characteristic of elemental selenium and selenium(−II) were observed, it can be deduced that the presence of Fe(II) traces as verified by UV−vis spectrophotometry did not lead to a significant amount (>2.5%) of reduced selenium.[33] Therefore, sorption was not accompanied by a significant reduction of selenium(IV) in contrast to Fe(II)-bearing minerals.[16]

Sorption samples at four different pH values (3.4, 4.0, 6.0, and 8.0) were analyzed by Se K-edge XAFS spectroscopy (Figure 3).

The Fourier transform magnitude is dominated by a strong peak at about 1.3 Å (uncorrected for phase shift), which arises from backscattering of the oxygen atoms in the coordination sphere. This peak was fitted with 3 Se-O paths with a length of 1.71 Å (Table 1), confirming the structure of the pyramidal selenite $Se^{IV}O_3$ unit.[60,61]

Beyond this coordination sphere, the signal intensity becomes very weak, but two peaks (depending on pH) clearly rise above the background noise level in the region beyond 3.5 Å. The first one at about 2.6 Å (labeled ES) is present for all four pH values, while the second at 2.9 Å (labeled CS) is present for the three more acidic samples, and seems to be absent at pH 8.0. The ES peak was fitted with 0.2 to 0.5 Fe atoms at distances of 2.88−2.91 Å. The CS peak was fitted with up to 1.3 Fe atoms at distances of 3.36−3.38 Å (Table 1). While such small coordination numbers have a large error and may appear statistically insignificant, they were necessary to obtain a satisfying fit of the spectra. Furthermore, they are supported by the factor analysis as shown further down.

While the fit with two Se-Fe paths provided consistent results, two alternative scenarios have to be considered. (1) For the SeO_3^{2-} ion, the Se-O double bond is fully delocalized, resulting in C_{3v} symmetry and three equal Se−O distances, while the $HSeO_3^-$ and $H_2SeO_3^0$ species have lower symmetry and Se−O distances varying by up to 0.05 Å.[60,62] In the case of the SeO_3^{2-} ion, a trilegged multiple scattering path Se−O−O about 3.0 Å in length may become significant, resulting in a 6-fold degeneracy for the C_{3v} symmetry, as has been also

dx.doi.org/10.1021/es4045852 | Environ. Sci. Technol. 2014, 48, 1665−1674

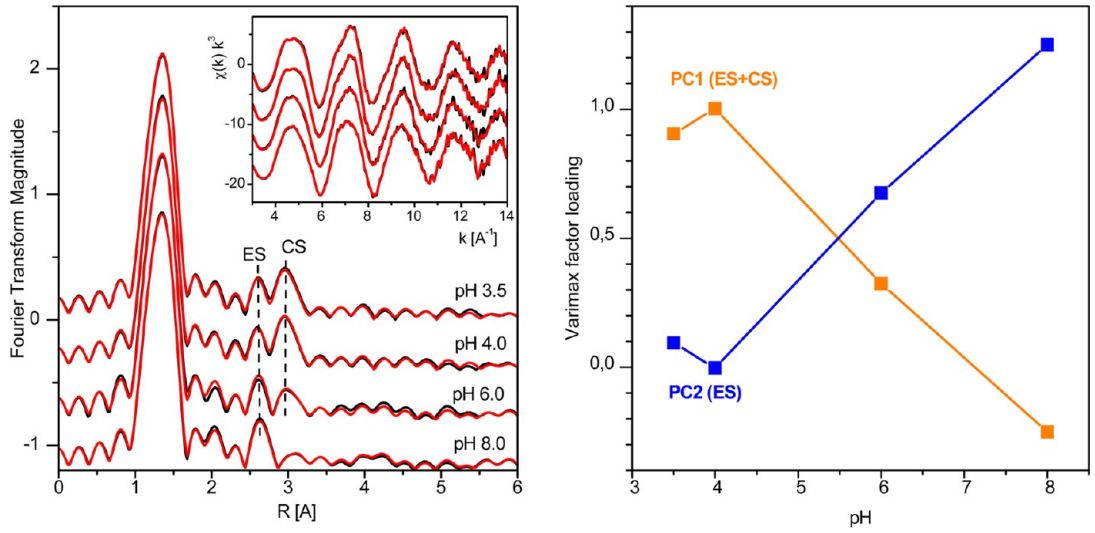

Figure 3. Se K-edge EXAFS spectra of Se(IV) sorbed to maghemite. Left: Experimental spectra (black lines) and their reconstruction by two factors (red lines) shown as Fourier Transform and k^3-weighted χ spectra (insert). Right: Varimax loadings of the two factors, the first one predominating at low pH representing both edge- and corner-sharing complexes, the second one predominating at high pH representing only the edge-sharing complex.

Table 1. Se-K EXAFS Fit Results of Se(IV)-Sorbed Maghemite (Amplitude Reduction Factor S_0^2 = 0.9)

	oxygen shell			iron shells			ΔE_0 [eV]	χ^2_{res} %
pH	CN[a]	R [Å][b]	σ^2 [Å²][c]	CN	R [Å]	σ^2 [Å²]		
3.5	3.0	1.71	0.0020	0.5	2.91	0.0077	17.0	13.0
				1.3	3.38	0.0065		
4.0	2.9	1.71	0.0015	0.2	2.91	0.0024	16.3	15.1
				1.2	3.38	0.0055		
6.0	3.0	1.71	0.0018	0.2	2.89	0.0021	16.2	14.9
				0.5	3.36	0.0040		
8.0	2.9	1.71	0.0020	0.5	2.88	0.0046	16.7	14.1

[a]CN: coordination number, error ± 25% [b]R: radial distance, error ± 0.01 Å [c]σ^2: Debye–Waller factor, error ± 0.0005 Å²

observed for other oxyanions such as arsenic(V).[63] (2) The ES peak could also arise from a Se–O single-scattering path about 2.9 Å in length, occurring in selenite solids. A wavelet analysis of the 2.5 to 3.5 Å region, however, did not reveal significant contributions of lighter atoms besides the heavier Fe.[64] Furthermore, by considering these two additional paths during the shell fit, neither significant contribution to the "ES" FT peak, nor changes in the fit parameters of the Se–Fe shell appeared. They were consequently omitted. The absence of the trilegged multiple scattering path points to a deviation from the C_{3v} symmetry, induced by the surface complexation.

The shorter Se–Fe distance of 2.9 Å is in line with a bidentate mononuclear edge-sharing (^{1}E) linkage between one SeO_3^{2-} pyramid and one FeO_6 octahedron, as e.g., in the structure of the solid $Fe_3(H_2O)(SeO_3)_3$.[65] The longer Se–Fe distance of 3.37 Å is in line with a bidentate binuclear corner-sharing (^{2}C) linkage between one SeO_3^{2-} pyramid and two FeO_6 octahedra.[65] The even longer Se–Fe distances ≥ 3.5 Å of monodentate mononuclear corner-sharing complexes (^{1}V) could not be fitted, indicating that they occur only in negligible proportions, if at all. The small coordination numbers exclude formation of precipitates.

On the basis of EXAFS studies, the coexistence of bidentate mononuclear edge-sharing (^{1}E) and bidentate binuclear corner-sharing (^{2}C) inner-sphere selenite surface complexes on Hydrous Ferric Oxide (HFO) was suggested,[40] while only the bidentate binuclear corner-sharing (^{2}C) complex was consistently observed on goethite.[39,40,66] According to Manceau and Charlet,[40] the presence of additional bidentate mononuclear edge sharing (^{1}E) surface complex onto HFO was due to structural differences between goethite and HFO (different proportion of edge termination on both solids). From IR studies on air-dried goethite and air-dried am-Fe(OH)$_3$, Su and Suarez[41] suggested that sorption of selenite leads to the formation of bidentate bridging surface complex.

Former studies highlighted the influence of surface loading on the coordination fashion of oxyanions onto iron oxides. Fendorf et al.[67] examined by XAS the sorption of AsO_4^{3-} onto goethite according to the surface loading (arising from different pH). The formation of monodentate complex was favored at low surface coverage, while formation of a bidentate–binuclear complex and bidentate–mononuclear complex was observed at higher surface coverage (the bidentate–binuclear complex was the predominant one for high surface loadings).[67] Missana et al.,[66] who studied selenite sorption onto magnetite by EXAFS, observed that the ^{1}E surface complex was favored at low surface loading (i.e., at pH 9.4), while a mixture of ^{1}E and ^{2}C complexes appeared at higher surface loading (i.e., pH 6.4).

In our study, we observe that the bidentate mononuclear edge-sharing ^{1}E complex prevails at pH 8, while at lower pH, both complexes occur. Not surprising due to their relatively high uncertainty, the Se–Fe coordination numbers do not show a clear trend with pH. However, the FT peaks suggest that ^{2}C becomes more important for the samples at pH 3.5 and 4.0 in comparison to the sample at pH 6.0, where the ^{1}E peak height seems to be higher (Figure 3). To follow this trend more systematically, we applied factor analysis.[16,45] The close match between the experimental spectra (black in Figure 3) and their reconstruction by two factors (red) demonstrates that two structural entities or species are present in all four samples. The Varimax factor loading confirms that the samples at pH 3.5–4.0

dx.doi.org/10.1021/es4045852 | Environ. Sci. Technol. 2014, 48, 1665–1674

and at pH 8.0 constitute extremes; however, only sample pH 8.0 with ^{1}E configuration represents a limiting species, while the samples at pH 3.5 and 4.0 contain a mixture of both species. The factor loadings further validate the visual impression that the sample at pH 6 represents an intermediate in speciation, with a higher ratio of ^{1}E over ^{2}C. Reasons for such pH-dependent transition will be given in the following section.

While this is to the best of our knowledge, the first molecular study of selenite sorption to maghemite, previous studies were conducted on selenite sorption to magnetite. Due to its Fe(II) content and low bandgap, magnetite reduced selenite to the −II oxidation state.[16,64] However, in the study of Missana et al.,[66] no reduction occurred, and in this case, the transition from solely ^{1}E to a mixture of ^{1}E and ^{2}C complexes with increasing surface loading (decreasing pH) was also observed, similarly to our results.

However, we cannot definitely rule out the presence of outer-sphere complexes during selenium(IV) sorption onto maghemite. Indeed, it is difficult by EXAFS to detect the occurrence of outer-sphere surface complexes in the simultaneous presence of inner-sphere surface complexes.[68] The ability of resonant anomalous X-ray reflectivity (RAXR) and Grazing-Incidence X-ray absorption fine structure (GI-XAFS) spectroscopy to observe outer-sphere complexes during sorption processes was evidenced by Catalano et al.[69] and Bargar et al.,[70] as recently highlighted.[68] Indeed, Catalano et al.[69] showed, for the first time, by using RAXR the presence of outer-sphere complexes (probably hydrogen-bonded species) in addition to inner-sphere ^{2}C complexes upon As(V) sorption onto corundum and hematite (012) surfaces. In addition, GI-XAFS was used by Bargar et al.[70] to study the adsorption of Pb(II) onto α-Al_2O_3 (0001) single crystal surface (although data were not corrected for polarization effects, which may question the numbers of reported Al(III) neighbors and interatomic distances).

Comparison between Se(IV) Uptake onto Magnetite and Maghemite. It is worthwhile comparing the sorption reactivity of selenium(IV) at the γ-Fe_2O_3 and Fe_3O_4 surface. Indeed, the structures of magnetite and maghemite are deeply correlated. Magnetite ($(Fe^{III})_A[Fe^{II}Fe^{III}]_BO_4$) is an inverse cubic spinel belonging to the space group Fd3m. In contrast, maghemite ($(Fe^{III})_A[Fe^{III}_{5/3\square 1/3}]_BO_4$) is a fully oxidized iron oxide, i.e., all the iron is in the +III oxidation state.[20] The crystal structure of maghemite is strictly related to the inverse spinel structure of magnetite (Fe_3O_4), but the difference arises from the presence of vacancies in the cation sublattice.[71−74]

A recent study performed by Petitto et al.,[75] based on crystal truncation rod diffraction data established on orientated magnetite single crystal, revealed that the most predominant (111) facets of the hydrated magnetite surface consists of two chemically inequivalent oxygen terminated domains: 75% of octahedral iron domains and 25% of mixed tetrahedral-octahedral iron domains. The octahedral termination was found to be dominant and therefore to control the reactivity at the hydrated Fe_3O_4(111)/water interfaces. In addition, Petitto et al.[75] study's revealed the presence of vacant tetrahedral iron sites in the mixed tetrahedral-octahedral iron termination. Unfortunately, the authors are not aware of such studies concerning maghemite hydrated layer.

In our study, we observed the transition from solely ^{1}E to a mixture of ^{1}E and ^{2}C complexes with increasing surface loading (decreasing pH), in agreement with Missana et al.[66] observations onto nano magnetite particles (nanocrystals (50−200 nm)), confirming the crystal similarity between both maghemite and magnetite surfaces.

According to literature, based on the Wulf theorem and morphology studies (TEM and SEM), the magnetite and maghemite nanoparticles with a cubic symmetry expose predominantly the {111}, {110}, and {100} low-index and low energy crystallographic planes, which are the three densest lattice planes.[76,77] The morphology of our commercial nanosized γ-Fe_2O_3 particles was observed by TEM. In particular, Figure 4 shows an HRTEM image of a maghemite

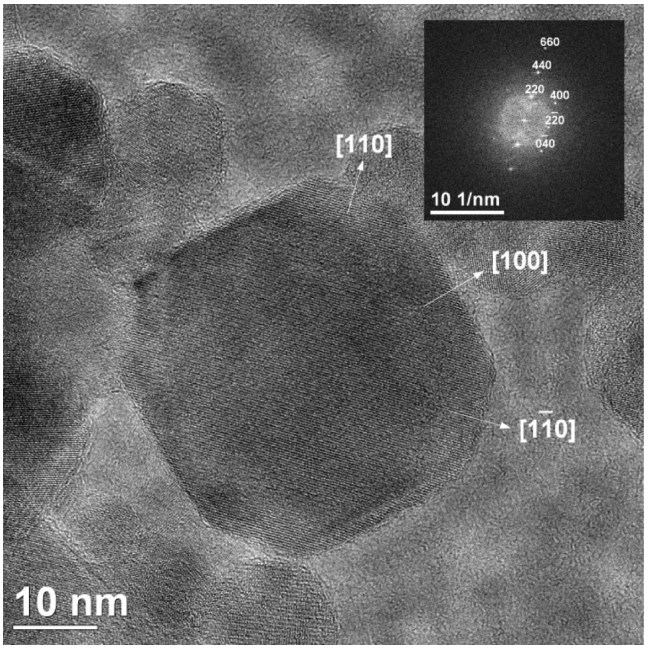

Figure 4. HRTEM image of an γ-Fe_2O_3 nanoparticle along the [100] zone axis together with its Fourier transform indexed based on the cubic structure of maghemite.

nanoparticle. Fourier transformation of the corresponding part of the high-resolution electron micrograph indicates, that the nanoparticle is oriented along the [100] zone axis and exhibits {100} and {110} facets. The {111} facets are not observed in Figure 4. They would be inclined to the [100] zone axis by 54.7°.

On the basis of structural information,[76,78,79] a scheme representing the crystalline structure of maghemite (Figure 5) containing the three main lattices was drawn.

In agreement with Wang et al.,[78,79] it becomes obvious that the formation of bidentate binuclear ^{2}C complex on the octahedral surface termination of the {111} facet of maghemite is not possible since adjacent iron octahedra do not show the required singly coordinated oxygens for such complexation pathway.[78,79] However, such complexes can be formed on the {100} facet, where rows of octahedra with singly coordinated oxygens are clearly visible.[78] The formation of the second kind of surface complex, namely the bidentate mononuclear edge-sharing complex, is likely to occur on the {110} facet of maghemite (Figure 5). We hypothesize that edge sites, located, e.g., at the {110} facet, are high energy sites and active at low surface loading, while the formation of ^{2}C takes place at {100} facets having rows of octahedra with singly coordinated oxygens (low energy sites). This seems to be a reasonable explanation of the presence of a mix of bidentate mononuclear

dx.doi.org/10.1021/es4045852 | Environ. Sci. Technol. 2014, 48, 1665−1674

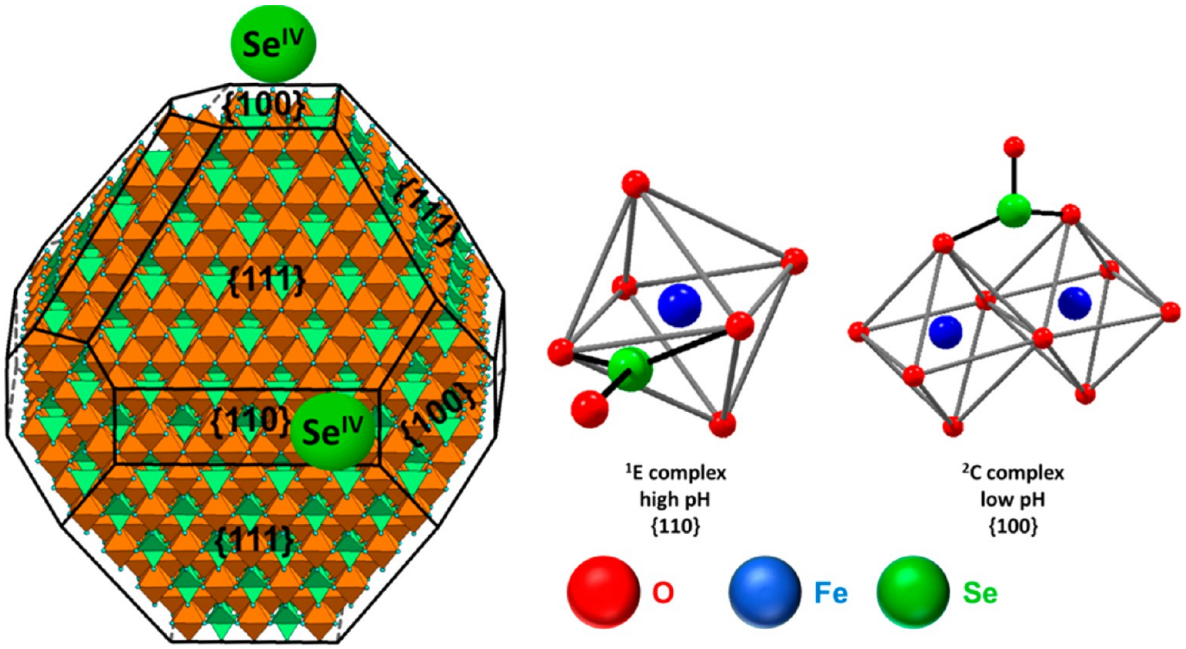

Figure 5. Scheme representing the crystalline structure of maghemite containing the three main lattices {111}, {110}, and {100} and the two observed ^{1}E and ^{2}C surface complexes.

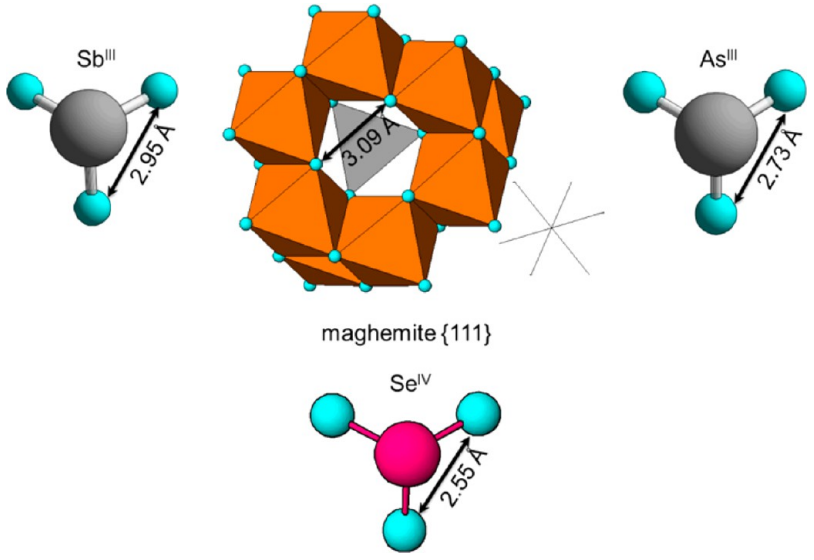

Figure 6. Scheme representing the Sb(III), As(III) and Se(IV) oxyanions and their compatibility/incompatibility toward vacant FeO_4 tetrahedral sites of the {111} maghemite facet.

edge-sharing (^{1}E) and bidentate binuclear corner-sharing (^{2}C) complexes whose proportion change upon surface loading. Note that the formation of ^{1}E complexes could also alternatively take place at the {111} facet or at edges between {111} and {100} or {110} facets.[80] Surface charge effects, which may be distinct for each facet, could be another possibility to explain the relative proportion of inner-sphere complexes. To get further information, Resonant Anomalous X-ray Reflectivity[69] or Crystal truncation rod diffraction[75] on maghemite could be excellent methods, but require single crystals.

Comparison between As(III), Sb(III) and Se(IV) Uptake onto Magnetite and Maghemite. It was recently shown that both magnetite and maghemite are able to sorb AsO_3^{3-}, $Sb(OH)_3$, and SeO_3^{2-}.[29,76,79,81] Since all of these three oxyanions adopt a pyramidal structure with a C_{3v} symmetry, the comparison of their behavior might highlight interesting differences.

The presence of different sorption sites onto the surface of maghemite was already suggested by Morin et al.,[29] who observed a mix of ^{2}C, ^{2}E, and ^{1}V As(III) inner-sphere surface complexes. Indeed, the authors highlighted an indirect evidence of a structural disorder on the maghemite (111) surface [based on a range of As-Fe distances (2.9−3.5 Å) observed by EXAFS spectroscopy (Table 1)]. One could get a great benefit from information about the structure of the hydrated maghemite, the reactive sites at the water interface as well as hydration shell network organization. Again, a detailed knowledge of the surface of hydrated maghemite is, as far as we know, unfortunately not available in the literature.

dx.doi.org/10.1021/es4045852 | Environ. Sci. Technol. 2014, 48, 1665−1674

Auffan et al.[76] studied the sorption of As(III) onto ultrafine maghemite nanoparticles (~6 nm in diameter) and reported the formation of tridentate hexanuclear corner-sharing (^{3}C) inner-sphere complexes onto maghemite (111) surface. These unusual arsenite $As^{III}O_3$ species were also observed during coprecipitation with nanomagnetite[79] and sorption of As(III) onto nanomagnetite.[82] As(III) was found to occupy vacant FeO_4 tetrahedral sites on octahedrally terminated (111) surfaces of magnetite.[79,82] A similar complex was found for Sb(III) sorption to magnetite.[81]

The question arises why such tridentate hexanuclear corner-sharing complexes (^{3}C) were not observed during Se(IV) sorption onto our commercial maghemite particles. The distance between the pyramidal oxygen atoms of the selenite unit is smaller (~2.65 Å) than that of arsenite (~2.73 Å) and that of antimonite (~2.94 Å). The corresponding oxygen distances at the maghemite surface are ~3.05 Å and hence much larger. While part of the structural incompatibility can be accounted for by a stretching of the O−O distances by increasing the $O-Sb^{III}-O$ and $O-As^{III}-O$ angles, this is evidently not possible any more for the smallest pyramidal unit of $Se^{IV}O_3$. Therefore, the absence of trilegged corner-sharing complexes for selenite reacted maghemite on the (111) surface may be explained by the incompatible structures (Figure 6).

■ ENVIRONMENTAL RELEVANCE

Due to aerial oxidation, nanomagnetite particles used for decontamination processes of air equilibrated waters may involve coating layers of maghemite, which will control the reactivity at the solid−water interface.[29] Magnetite and maghemite are both ferromagnetic[20] and show similar bulk saturation magnetization.[29] Both spinel phases exhibit magnetic properties, which ease their recovery by the application of an external magnetic field and allows in situ site-specific targeting.[83] In this study, it was shown that maghemite nanoparticles exhibited fast adsorption kinetics toward selenium(IV) due to their high surface area to volume ratio. At 2 g L^{-1} (data not shown), the use of maghemite enabled to achieve final concentration < 40 μg L^{-1} from solutions containing either 800 or 4000 μg L^{-1} Se(IV) and therefore to respect the guideline recommended by the WHO.[11] Note that the possibility to produce ultrafine (6 nm diameter) nanomaghemite particles with a specific surface area of 172 m^2 g^{-1} was already highlighted.[76] This decrease in particle size should significantly improve maghemite retention capacities toward selenium(IV). In addition, maghemite particles are chemically stable[74,84] and can form very stable and concentrated aqueous dispersions, even at low pH.[27] The application of maghemite for the decontamination of mine water or mine drainage with typically low pH[26] should therefore be considered, either for in situ remediation, in packed bed adsorption configuration[83] or mixed together with magnetite.[85] Furthermore, the application of maghemite as the sorbing phase for pollutant removal in air-equilibrated waters would not require surface modification to stabilize the particles, as for magnetite.[86]

Our XAS spectroscopic results provide new detailed knowledge at the molecular level to improve surface complexation modeling and to predict the retention behavior of selenium(IV) by maghemite or magnetite covered with layers of maghemite. They allow constraining without ambiguity the surface complexes denticity/bidentate mononuclear edge-sharing (^{1}E) and bidentate binuclear corner-sharing (^{2}C) complexes, formed on two different facets of maghemite. These surface complexes observed for maghemite might also be the surface complexes forming on magnetite, before the interfacial reduction step to Se(−II).

■ ASSOCIATED CONTENT

Supporting Information

Detailed descriptions concerning reagents, sorption experiments, verification of Se oxidation state in the aqueous phase, electrophoretic mobility measurements, X-ray Photoelectron Spectroscopy, Transmission Electron Microscopy, and the structure of magnetite and maghemite. This material is available free of charge via the Internet at http://pubs.acs.org.

■ AUTHOR INFORMATION

Corresponding Author

*Phone: ++49 351 260 2148 (N.J.); ++33 476 88 2462 (A.C.S.). Fax: ++49 351 260 3664 (N.J.). E-mail: n.jordan@hzdr.de (N.J.); scheinost@esrf.fr (A.C.S.).

Author Contributions

The manuscript was written through the contributions of all authors. All authors have given approval to the final version of the manuscript.

Funding

Funds were supplied by the German Federal Ministry of Economics and Technology (BMWi) through Contract No. 02E10790 for the VESPA Project.

Notes

The authors declare no competing financial interest.

■ ACKNOWLEDGMENTS

This work is part of the VESPA project, funded by the German Federal Ministry of Economics and Technology (BMWi) through Contract No. 02E10790. The authors would like to thank Christa Müller for her technical assistance for sorption experiments and electrophoretic mobility measurements, Ursula Schaefer for ICP-MS measurements, as well as Carola Eckardt for BET determination. We are grateful to Dr. Dipanjan Banerjee, Dr. Christoph Hennig, and Dr. André Rossberg for their experimental support during XAS measurements. The authors also want to acknowledge the Associate Editor as well as four anonymous reviewers for their constructive comments and suggestions.

■ REFERENCES

(1) Fordyce, F. Selenium geochemistry and health. *Ambio* **2007**, *36* (1), 94−97.

(2) Burau, R. G. Environmental chemistry of selenium. *Calif. Agr.* **1985**, *39* (7), 16−18.

(3) Conde, J. E.; Alaejos, M. S. Selenium concentrations in natural and environmental waters. *Chem. Rev.* **1997**, *97* (6), 1979−2003.

(4) Lemly, A. D. Guidelines for evaluating selenium data from aquatic monitoring and assessment studies. *Environ. Monit. Assess.* **1993**, *28* (1), 83−100.

(5) Ohlendorf, H. M.; Hoffman, D. J.; Saiki, M. K.; Aldrich, T. W. Embryonic mortality and abnormalities of aquatic birds—Apparent impacts of selenium from irrigation drainwater. *Sci. Total Environ.* **1986**, *52* (1−2), 49−63.

(6) Presser, T. S.; Ohlendorf, H. M. Biogeochemical cycling of selenium in the San-Joaquin valley, California, USA. *Environ. Manage.* **1987**, *11* (6), 805−821.

(7) Jörg, G.; Buhnemann, R.; Hollas, S.; Kivel, N.; Kossert, K.; Van Winckel, S.; Gostomski, C. L. V. Preparation of radiochemically pure Se-79 and highly precise determination of its half-life. *Appl. Radiat. Isot.* **2010**, *68* (12), 2339−2351.

(8) ANDRA. *Synthèse: Evaluation de la Faisabilité du Stockage Géologique en Formation Argileuse*; Agence Nationale pour la gestion des Déchets Radioactifs: Châtenay-Malabry, 2005.
(9) Brasser, T.; Droste, J.; Müller-Lyda, I.; Neles, J.; Sailer, M.; Schmidt, G.; Steinhoff, M. *Endlagerung Wärmeentwickelnder Radioaktiver Abfälle in Deutschland*;Gesellschaft für Anlagen und Reaktorsicherheit (GRS) mbH and Öko-Institut e.V.: Braunschweig/Darmstadt, 2008; *GRS-247*, ISBN 978-3-939355-22-9.
(10) ONDRAF/NIRAS. *Technical Overview of the SAFIR 2 Report—Safety Assessment and Feasibility Interim Report 2 (NIROND 2001−05 E)*; Belgian Agency for Radioactive Waste and Enriched Fissile Materials: Brussels, 2001.
(11) *Selenium in Drinking-Water. Background Document for Development of WHO Guidelines for Drinking-Water Quality*; World Health Organization, 2011.
(12) Hasan, S. H.; Ranjan, D.; Talat, M. Agro-industrial waste "wheat bran" for the biosorptive remediation of selenium through continuous up-flow fixed-bed column. *J. Hazard. Mater.* **2010**, *181* (1−3), 1134−1142.
(13) Liu, R.; Frost, R. L.; Martens, W. N. Absorption of the selenite anion from aqueous solutions by thermally activated layered double hydroxide. *Water Res.* **2009**, *43* (5), 1323−1329.
(14) Duc, M.; Lefevre, G.; Fedoroff, M. Sorption of selenite ions on hematite. *J. Colloid Interface Sci.* **2006**, *298* (2), 556−563.
(15) Elzinga, E. J.; Tang, Y. Z.; McDonald, J.; DeSisto, S.; Reeder, R. J. Macroscopic and spectroscopic characterization of selenate, selenite, and chromate adsorption at the solid−water interface of γ-Al_2O_3. *J. Colloid Interface Sci.* **2009**, *340* (2), 153−159.
(16) Scheinost, A. C.; Charlet, L. Selenite reduction by mackinawite, magnetite and siderite: XAS characterization of nanosized redox products. *Environ. Sci. Technol.* **2008**, *42* (6), 1984−1989.
(17) Jordan, N.; Foerstendorf, H.; Weiß, S.; Heim, K.; Schild, D.; Brendler, V. Sorption of selenium(VI) onto anatase: Macroscopic and microscopic characterization. *Geochim. Cosmochim. Acta* **2011**, *75*, 1519−1530.
(18) Barron, V.; Torrent, J.; de Grave, E. Hydromaghemite, an intermediate in the hydrothermal transformation of 2-line ferrihydrite into hematite. *Am. Mineral.* **2003**, *88* (11−12), 1679−1688.
(19) Batista, M. A.; da Costa, A. C. S.; Bigham, J. M.; de Santana, H.; Zaia, D. A. M.; de Souza, I. G. Mineralogical, chemical, and physical characterization of synthetic Al-substituted maghemites (γ-$Fe_{2-x}Al_xO_3$). *Clay Clay Miner.* **2010**, *58* (4), 451−461.
(20) Cornell, R. M.; Schwertmann, U. *The Iron Oxides: Structure, Properties, Reactions, Occurrences, and Uses*; Wiley-VCH: New York, 2003.
(21) Vandenberghe, R. E.; Barrero, C. A.; da Costa, G. M.; Van San, E.; De Grave, E. Mossbauer characterization of iron oxides and (oxy)hydroxides: The present state of the art. *Hyperfine Interact.* **2000**, *126* (1−4), 247−259.
(22) Ben Lagha, S.; Crusset, D.; Mabille, I.; Tran, M.; Bernard, M. C.; Sutter, E. Corrosion of iron: A study for radioactive waste canisters. *J. Nucl. Mater.* **2007**, *362* (2−3), 485−492.
(23) Antony, H.; Perrin, S.; Dillmann, P.; Legrand, L.; Chausse, A. Electrochemical study of indoor atmospheric corrosion layers formed on ancient iron artefacts. *Electrochim. Acta* **2007**, *52* (27), 7754−7759.
(24) Chitty, W. J.; Dillmann, P.; L'Hostis, V.; Lombard, C. Long-term corrosion resistance of metallic reinforcements in concrete—A study of corrosion mechanisms based on archaeological artefacts. *Corros. Sci.* **2005**, *47* (6), 1555−1581.
(25) Neff, D.; Dillmann, P.; Bellot-Gurlet, L.; Beranger, G. Corrosion of iron archaeological artefacts in soil: Characterisation of the corrosion system. *Corros. Sci.* **2005**, *47* (2), 515−535.
(26) Wei, X. C.; Bhojappa, S.; Lin, L. S.; Viadero, R. C. Performance of nano-magnetite for removal of selenium from aqueous solutions. *Environ. Eng. Sci.* **2012**, *29* (6), 526−532.
(27) Jolivet, J. P.; Chaneac, C.; Tronc, E. Iron oxide chemistry. From molecular clusters to extended solid networks. *Chem. Commun.* **2004**, 481−487.
(28) Tang, J.; Myers, M.; Bosnick, K. A.; Brus, L. E. Magnetite Fe_3O_4 nanocrystals: Spectroscopic observation of aqueous oxidation kinetics. *J. Phys. Chem. B* **2003**, *107* (30), 7501−7506.
(29) Morin, G.; Ona-Nguema, G.; Wang, Y. H.; Menguy, N.; Juillot, F.; Proux, O.; Guyot, F.; Calas, G.; Brown, G. E. Extended X-ray absorption fine structure analysis of arsenite and arsenate adsorption on maghemite. *Environ. Sci. Technol.* **2008**, *42* (7), 2361−2366.
(30) Afkhami, A.; Moosavi, R. Adsorptive removal of Congo red, a carcinogenic textile dye, from aqueous solutions by maghemite nanoparticles. *J. Hazard. Mater.* **2010**, *174* (1−3), 398−403.
(31) Afkhami, A.; Norooz-Asl, R. Removal, preconcentration and determination of Mo(VI) from water and wastewater samples using maghemite nanoparticles. *Colloids Surf. A-Physicochem. Eng. Asp.* **2009**, *346* (1−3), 52−57.
(32) Hu, J.; Chen, G. H.; Lo, I. M. C. Selective removal of heavy metals from industrial wastewater using maghemite nanoparticle: Performance and mechanisms. *J. Environ. Eng.-ASCE* **2006**, *132* (7), 709−715.
(33) Jordan, N.; Ritter, A.; Foerstendorf, H.; Scheinost, A. C.; Weiss, S.; Heim, K.; Grenzer, J.; Mucklich, A.; Reuther, H. Adsorption mechanism of selenium(VI) onto maghemite. *Geochim. Cosmochim. Acta* **2013**, *103*, 63−75.
(34) Nassar, N. N. Kinetics, mechanistic, equilibrium, and thermodynamic studies on the adsorption of acid red dye from wastewater by γ-Fe_2O_3 nanoadsorbents. *Sep. Sci. Technol.* **2010**, *45* (8), 1092−1103.
(35) Park, H.; Myung, N. V.; Jung, H.; Choi, H. As(V) remediation using electrochemically synthesized maghemite nanoparticles. *J. Nanopart. Res.* **2009**, *11* (8), 1981−1989.
(36) Tuutijärvi, T.; Lu, J.; Sillanpaa, M.; Chen, G. As(V) adsorption on maghemite nanoparticles. *J. Hazard. Mater.* **2009**, *166* (2−3), 1415−1420.
(37) Jiang, W.; Pelaez, M.; Dionysiou, D. D.; Entezari, M. H.; Tsoutsou, D.; O'Shea, K. Chromium(VI) removal by maghemite nanoparticles. *Chem. Eng. J.* **2013**, *222*, 527−533.
(38) Foster, A. L.; Brown, G. E.; Parks, G. A. X-ray absorption fine structure study of As(V) and Se(IV) sorption complexes on hydrous Mn oxides. *Geochim. Cosmochim. Acta* **2003**, *67* (11), 1937−1953.
(39) Hayes, K. F.; Roe, A. L.; Brown, G. E.; Hodgson, K. O.; Leckie, J. O.; Parks, G. A. In situ X-ray absorption study of surface complexes: Selenium oxyanions on α-FeOOH. *Science* **1987**, *238* (4828), 783−786.
(40) Manceau, A.; Charlet, L. The mechanism of selenate adsorption on goethite and hydrous ferric-oxide. *J. Colloid Interface Sci.* **1994**, *168* (1), 87−93.
(41) Su, C. M.; Suarez, D. L. Selenate and selenite sorption on iron oxides: An infrared and electrophoretic study. *Soil Sci. Soc. Am. J.* **2000**, *64* (1), 101−111.
(42) Webb, S. M. SIXpack: A graphical user interface for XAS analysis using IFEFFIT. *Phys. Scr.* **2005**, *T115*, 1011−1014.
(43) Ressler, T. WinXAS: A program for X-ray absorption spectroscopy data analysis under MS-Windows. *J. Synchrot. Radiat.* **1998**, *5*, 118−122.
(44) Ankudinov, A. L.; Rehr, J. J. Relativistic calculations of spin-dependent x-ray-absorption spectra. *Phys. Rev. B* **1997**, *56* (4), R1712−R1715.
(45) Rossberg, A.; Reich, T.; Bernhard, G. Complexation of uranium(VI) with protocatechuic acid—Application of iterative transformation factor analysis to EXAFS spectroscopy. *Anal. Bioanal. Chem.* **2003**, *376* (5), 631−638.
(46) Funke, H.; Scheinost, A. C.; Chukalina, M. Wavelet analysis of extended x-ray absorption fine structure data. *Phys. Rev. B* **2005**, *71* (9), 94110−1−94110−7.
(47) Jordan, N.; Lomenech, C.; Marmier, N.; Giffaut, E.; Ehrhardt, J. J. Sorption of selenium(IV) onto magnetite in the presence of silicic acid. *J. Colloid Interface Sci.* **2009**, *329* (1), 17−23.
(48) Jordan, N.; Marmier, N.; Lomenech, C.; Giffaut, E.; Ehrhardt, J. J. Competition between selenium (IV) and silicic acid on the hematite surface. *Chemosphere* **2009**, *75* (1), 129−134.

(49) Rovira, M.; Gimenez, J.; Martinez, M.; Martinez-Llado, X.; de Pablo, J.; Marti, V.; Duro, L. Sorption of selenium(IV) and selenium(VI) onto natural iron oxides: Goethite and hematite. *J. Hazard. Mater.* **2008**, *150* (2), 279−284.
(50) Balistrieri, L. S.; Chao, T. T. Selenium adsorption by goethite. *Soil Sci. Soc. Am. J.* **1987**, *51* (5), 1145−1151.
(51) Parida, K. M.; Gorai, B.; Das, N. N.; Rao, S. B. Studies on ferric oxide hydroxides 0.3. Adsorption of selenite (SeO_3^{2-}) on different forms of iron oxyhydroxides. *J. Colloid Interface Sci.* **1997**, *185* (2), 355−362.
(52) Dash, S. S.; Parida, K. M. Studies on selenite adsorption using manganese nodule leached residues. *J. Colloid Interface Sci.* **2007**, *307* (2), 333−339.
(53) Stumm, W.; Huang, C. P.; Jenkins, S. R. Specific chemical interaction affecting stability of dispersed systems. *Croat. Chem. Acta* **1970**, *42* (2), 223−245.
(54) Duc, M.; Lefevre, G.; Fedoroff, M.; Jeanjean, J.; Rouchaud, J. C.; Monteil-Rivera, F.; Dumonceau, J.; Milonjic, S. Sorption of selenium anionic species on apatites and iron oxides from aqueous solutions. *J. Environ. Radioact.* **2003**, *70* (1−2), 61−72.
(55) Shi, K. L.; Wang, X. F.; Guo, Z. J.; Wang, S. G.; Wu, W. S. Se(IV) sorption on TiO_2: Sorption kinetics and surface complexation modeling. *Colloids Surf. A-Physicochem. Eng. Asp.* **2009**, *349* (1−3), 90−95.
(56) Boguslavsky, Y.; Margel, S. Synthesis and characterization of poly (divinylbenzene)-coated magnetic iron oxide nanoparticles as precursor for the formation of air-stable carbon-coated iron crystalline nanoparticles. *J. Colloid Interface Sci.* **2008**, *317* (1), 101−114.
(57) Mornet, S.; Portier, J.; Duguet, E. A method for synthesis and functionalization of ultrasmall superparamagnetic covalent carriers based on maghemite and dextran. *J. Magn. Magn. Mater.* **2005**, *293* (1), 127−134.
(58) Tuutijärvi, T.; Lu, J.; Sillanpaa, M.; Chen, G. Adsorption mechanism of arsenate on crystal γ-Fe_2O_3 nanoparticles. *J. Environ. Eng.-ASCE* **2010**, *136* (9), 897−905.
(59) Yu, S.; Chow, G. M. Carboxyl group ($-CO_2H$) functionalized ferrimagnetic iron oxide nanoparticles for potential bio-applications. *J. Mater. Chem.* **2004**, *14* (18), 2781−2786.
(60) Peak, D.; Saha, U. K.; Huang, P. M. Selenite adsorption mechanisms on pure and coated montmorillonite: An EXAFS and XANES spectroscopic study. *Soil Sci. Soc. Am. J.* **2006**, *70*, 192−203.
(61) Charlet, L.; Scheinost, A. C.; Tournassat, C.; Greneche, J. M.; Gehin, A.; Fernandez-Martinez, A.; Coudert, S.; Tisserand, D.; Brendle, J. Electron transfer at the mineral/water interface: Selenium reduction by ferrous iron sorbed on clay. *Geochim. Cosmochim. Acta* **2007**, *71* (23), 5731−5749.
(62) Valkonen, J.; Koskenlinna, M. The crystal structure of iron(III) hydrogen biselenite, $FeH(SeO_3)_2$. *Acta Chem. Scand. A* **1978**, *32*, 603−606.
(63) Sherman, D. M.; Randall, S. R. Surface complexation of arsenic(V) to iron(III) (hydr)oxides: Structural mechanism from ab initio molecular geometries and EXAFS spectroscopy. *Geochim. Cosmochim. Acta* **2003**, *67* (22), 4223−4230.
(64) Scheinost, A. C.; Kirsch, R.; Banerjee, D.; Fernandez-Martinez, A.; Zänker, H.; Funke, H.; Charlet, L. X-ray absorption and photoelectron spectroscopy investigation of selenite reduction by Fe^{II}-bearing minerals. *J. Contam. Hydrol.* **2008**, *102*, 228−245.
(65) Xiao, D. R.; Hou, Y.; Wang, E. B.; An, H. Y.; Lu, H.; Li, Y. G.; Xu, L.; Hu, C. W. Hydrothermal synthesis and crystal structure of a three-dimensional metal selenite containing double helical chains: $Fe_3(H_2O)(SeO_3)_3$. *J. Solid State Chem.* **2004**, *177* (8), 2699−2704.
(66) Missana, T.; Alonso, U.; Scheinost, A. C.; Granizo, N.; Garcia-Gutierrez, M. Selenite retention by nanocrystalline magnetite: Role of adsorption, reduction and dissolution/co-precipitation processes. *Geochim. Cosmochim. Acta* **2009**, *73* (20), 6205−6217.
(67) Fendorf, S.; Eick, M. J.; Grossl, P.; Sparks, D. L. Arsenate and chromate retention mechanisms on goethite 0.1. Surface structure. *Environ. Sci. Technol.* **1997**, *31* (2), 315−320.
(68) Charlet, L.; Morin, G.; Rose, J.; Wang, Y. H.; Auffan, M.; Burnol, A.; Fernandez-Martinez, A. Reactivity at (nano)particle-water interfaces, redox processes, and arsenic transport in the environment. *C. R. Geosci.* **2011**, *343* (2−3), 123−139.
(69) Catalano, J. G.; Park, C.; Fenter, P.; Zhang, Z. Simultaneous inner- and outer-sphere arsenate adsorption on corundum and hematite. *Geochim. Cosmochim. Acta* **2008**, *72* (8), 1986−2004.
(70) Bargar, J. R.; Towle, S. N.; Brown, G. E.; Parks, G. A. Outer-sphere Pb(II) adsorbed at specific surface sites on single crystal alpha-alumina. *Geochim. Cosmochim. Acta* **1996**, *60* (18), 3541−3547.
(71) Belin, T.; Guigue-Millot, N.; Caillot, T.; Aymes, D.; Niepce, J. C. Influence of grain size, oxygen stoichiometry, and synthesis conditions on the γ-Fe_2O_3 vacancies ordering and lattice parameters. *J. Solid State Chem.* **2002**, *163* (2), 459−465.
(72) Jorgensen, J. E.; Mosegaard, L.; Thomsen, L. E.; Jensen, T. R.; Hanson, J. C. Formation of γ-Fe_2O_3 nanoparticles and vacancy ordering: An in situ X-ray powder diffraction study. *J. Solid State Chem.* **2007**, *180* (1), 180−185.
(73) Morales, M. P.; Pecharroman, C.; Carreno, T. G.; Serna, C. J. Structural characteristics of uniform γ-Fe_2O_3 particles with different axial (length/width) ratios. *J. Solid State Chem.* **1994**, *108* (1), 158−163.
(74) Serna, C. J.; Morales, M. P. Maghemite (γ-Fe_2O_3): A versatile magnetic colloidal material. *Surf. Colloid Sci.* **2004**, *17*, 27−81.
(75) Petitto, S. C.; Tanwar, K. S.; Ghose, S. K.; Eng, P. J.; Trainor, T. P. Surface structure of magnetite (111) under hydrated conditions by crystal truncation rod diffraction. *Surf. Sci.* **2010**, *604* (13−14), 1082−1093.
(76) Auffan, M.; Rose, J.; Proux, O.; Borschneck, D.; Masion, A.; Chaurand, P.; Hazemann, J. L.; Chaneac, C.; Jolivet, J. P.; Wiesner, M. R.; Van Geen, A.; Bottero, J. Y. Enhanced adsorption of arsenic onto maghemites nanoparticles: As(III) as a probe of the surface structure and heterogeneity. *Langmuir* **2008**, *24* (7), 3215−3222.
(77) Zhao, N.; Ma, W.; Cui, Z. M.; Song, W. G.; Xu, C. L.; Gao, M. Y. Polyhedral maghemite nanocrystals prepared by a flame synthetic method, preparations, characterizations, and catalytic properties. *ACS Nano* **2009**, 3 (7), 1775−1780.
(78) Wang, Y. H.; Morin, G.; Ona-Nguema, G.; Juillot, F.; Calas, G.; Brown, G. E. Distinctive arsenic(V) trapping modes by magnetite nanoparticles induced by different sorption processes. *Environ. Sci. Technol.* **2011**, *45* (17), 7258−7266.
(79) Wang, Y. H.; Morin, G.; Ona-Nguema, G.; Menguy, N.; Juillot, F.; Aubry, E.; Guyot, F.; Calas, G.; Brown, G. E. Arsenite sorption at the magnetite-water interface during aqueous precipitation of magnetite: EXAFS evidence for a new arsenite surface complex. *Geochim. Cosmochim. Acta* **2008**, *72* (11), 2573−2586.
(80) Dulnee, S.; Banerjee, D.; Merkel, B. J.; Scheinost, A. C. Surface complexation and oxidation of Sn^{II} by nanomagnetite. *Environ. Sci. Technol.* **2013**, *47*, 12852−12859.
(81) Kirsch, R.; Scheinost, A. C.; Rossberg, A.; Banerjee, D.; Charlet, L. Reduction of antimony by nano-particulate magnetite and mackinawite. *Mineral. Mag.* **2008**, *72* (1), 185−189.
(82) Morin, G.; Wang, Y. H.; Ona-Nguema, G.; Juillot, F.; Calas, G.; Menguy, N.; Aubry, E.; Bargar, J. R.; Brown, G. E. EXAFS and HRTEM evidence for As(III)-containing surface precipitates on nanocrystalline magnetite: Implications for as sequestration. *Langmuir* **2009**, *25* (16), 9119−9128.
(83) Nassar, N. N. Iron Oxide Nanoadsorbents for Removal of Various Pollutants from Wastewater: An Overview. In *Application of Adsorbents for Water Pollution Control*; Bhatnagar, A., Ed.; Bentham Science Publishers Ltd.: Sarjah, United Arab Emirates, 2012; pp 81−118.
(84) Machala, L.; Tucek, J.; Zboril, R. Polymorphous transformations of nanometric iron(III) oxide: A review. *Chem. Mater.* **2011**, *23*, 3255−3272.
(85) Chowdhury, S. R.; Yanful, E. K. Arsenic and chromium removal by mixed magnetite-maghemite nanoparticles and the effect of phosphate on removal. *J. Environ. Manage.* **2010**, *91* (11), 2238−2247.

(86) Carlos, L.; García Einschlag, F. S.; González, M. C.; Mártire, D. O. Applications of Magnetite Nanoparticles for Heavy Metal Removal from Wastewater. In *Waste Water—Treatment Technologies and Recent Analytical Developments*; García Einschlag, F. S.; Carlos, L., Eds.; InTech: Rijeka, Croatia, 2013.